A Novel Mono-energy Proton Arc Therapy with Patient Specific Range Shifter for Fast Treatment Delivery

by

Yuyin Zhou

DKU Medical Physics
Duke University

Defense Date: April 3, 2024

Approved:

Manju Liu, Co-Advisor

Fangfang Yin, Co-Advisor

Jianyue Jin

Gang Liu

Qiuwen Wu

Thesis submitted in partial fulfillment of the requirements for the degree of Master of Science in the Department of DKU Medical Physics in The Graduate School of Duke University
2024

ABSTRACT

A Novel Mono-energy Proton Arc Therapy with Patient Specific Range Shifter for Fast Treatment Delivery

by

Yuyin Zhou

DKU Medical Physics
Duke University

Defense Date: April 3, 2024

Approved:

Manju Liu, Co-Advisor

Fangfang Yin, Co-Advisor

Jianyue Jin

Gang Liu

Qiuwen Wu

Thesis submitted in partial fulfillment of the requirements for the degree of Master of Science in the Department of DKU Medical Physics in The Graduate School of Duke University
2024

Abstract

Introduction: This study evaluates a novel proton therapy filter that aims to decrease delivery time by eliminating the necessity for energy adjustments. Utilizing the machine's maximum energy, the filter structure was designed through optimization which ensures sufficient tumor coverage through the proton beam Bragg-peak. As a result, this innovation has the potential to improve treatment efficiency by shortening the delivery time.

Methods: Implemented on the matRad platform, each plan utilized a single arc composed of 72 beams, each spaced 5 degrees apart. Open-access datasets, including TG-119 C-shape, a prostate case, and a liver case, were employed. The prescribed doses for these cases were 50Gy in 25 fractions, 68Gy in 34 fractions, and 45Gy in 25 fractions, respectively. Simplifying from multiple energy delivery to a single energy delivery can reduce treatment delivery time. Maintaining spot coverage with a single energy layer for each beamlet is a critical optimization aspect. The spot coverage, P(i,j), is optimized to be maximized and the optimization is called Mono-energy optimization. However, considering spot coverage alone is insufficient; the energy level must also be considered. Higher energy level indicates a thinner range shifter, which reduces scatter and attenuation caused by range shifters.

The new optimization process, called Higher-mono-energy optimization, gave priority to deeper layers and larger spot sizes, using a function that normalizes input energy and combines it with alpha and beta coefficients to optimize the energy function E(i,j) and spot coverage P(i,j). The optimal energy layers were selected, and the initial beam energy was set at 236MeV. All beamlets were adjusted to specific energy levels with a custom-designed PMMA filter based on stopping power, facilitating a smooth transition to the desired energy levels. The effectiveness of this approach was evaluated by comparing dose metrics with those from the Intensity Modulated Proton Therapy (IMPT) method using two or three beams.

Results: PTV coverages were relatively close between the IMPT and range filter plans. Organs at Risk (OAR) experienced a dose increase due to enhanced scattering. Simulated treatment delivery times for the three tested range filter plans demonstrated the efficiency, with prostate at 360s, liver at 340s, and TG119 at 390s.

Conclusions: Mono-energy with range filters proton therapy is a feasible approach for expediting treatment delivery without compromising the quality of the treatment plan.

Dedication

First and foremost, I wish to express my sincere gratitude to my advisors, Prof. Manju Liu and Prof. Gang Liu, for their invaluable guidance and support. Their expertise and insight were crucial in overcoming the challenges I faced and in providing the clarity necessary to navigate the complexities of my academic thesis project. Their steadfast encouragement was a fundamental pillar of my journey, and for this, I am deeply thankful.

I am also greatly indebted to Prof. Fangfang Yin for his wise counsel. He imparted to me the understanding that the quest for perfection in research outcomes is secondary to the journey of discovery and learning from results, including those that challenge our initial hypotheses. His support was key in my continued commitment to the project.

My thanks extend to the faculty, staff, and fellow students of the Medical Physics program at Duke Kunshan University. The knowledge and life lessons I have gained during my tenure have been profoundly enriching and will be held in high regard.

I extend special thanks to the students in Prof. Gang Liu's group at Wuhan University. Their openness in sharing their research findings and their assistance with calculating delivery times have been invaluable contributions to my work.

I am grateful to all my committee members, Prof. Jianyue Jin and Prof. Qiuwen Wu, for their participation in my master's thesis defense. Their feedback and guidance have been immensely beneficial to me.

Lastly, but most importantly, I must convey my deepest appreciation to my family. Your constant support and faith in me have been the bedrock of my strength and motivation.

Contents

List of Tables

List of Figures

1. Introduction

1.1 Background

Cancer is the leading cause of death worldwide. The exact causes of cancer remain unclear, which complicates efforts to find effective treatments. Mainstream cancer treatments include chemotherapy, surgery, radiation therapy, immunotherapy, and hormonal therapy. Among these, radiation therapy plays a crucial role. Approximately 50% of cancer patients receive radiation therapy at some point during their treatment.

Radiation therapy can be applied at different stages of cancer treatment. When used before surgery, its goal is to reduce the size of the tumor. When applied after surgery, radiation therapy aims to destroy any microscopic cancer cells that remain and are invisible to the naked eye, thereby reducing the risk of tumor recurrence.

The goal of radiation therapy is to maximize the dose to tumor cells while minimizing exposure to normal tissue. The advantage of radiation therapy is non-invasive.[1]

1.2 Radiation

Radiation can be classified into two types: electromagnetic radiation and particulate radiation. Electromagnetic radiation includes X-ray, gamma ray, visible light and microwave, travelling at light speed. In the field of radiation therapy, X-ray and gamma ray are two major types of electromagnetic radiation. X-ray and gamma ray used in radiation therapy have enough energy to ionize water component to create free radicals, which can cause indirect damage on DNA. Particulate radiation includes electron, proton and neutron, etc. Particles have rest mass at high speed, and they can directly interact with DNA and cause damage. [1,2]

High-energy photon beams can deliver the maximum dose at a specific depth. Higher energy photon beam allows for deeper penetration into tumors while preserving the skin, known

as the skin sparing effect. Intensity Modulated Radiation Therapy represents the current standard RT technique, offering precise dose distribution that better spares surrounding healthy tissue.

Electron therapy is particularly effective for treating superficial tumors, such as malignant melanoma, head-and-neck cancer, postmastectomy radiotherapy, etc. [5]

Proton therapy has demonstrated its advantage in treating head and neck cancer as well as pediatric tumors. [6]

1.3 Proton therapy physics

Protons are positively charged particles with a mass 1836 times greater than that of electrons, and they have a significant rest mass. As they pass through material, their energy continuously decreases. The rate of energy loss per unit path length is known as stopping power, which refers to the capability of depositing energy per unit length in matter. The stopping power will increase as the protons slow down. When the energy of protons approaches zero, its stopping power reaches a peak, indicating the maximum energy deposition in the matter and there is a dose peak at the end of the proton range. The dose peak is known as Bragg Peak. After this peak, the dose drops sharply to almost zero, no exit dose. However, single Bragg peak is narrow. To cover the entire target, a spread out Bragg peak (SOBP) is created. SOBP is produced by combining multiple energy proton beams. The surface dose of SOBP is not as low as single Bragg peak. The dose distribution of photon, proton is shown in Figure 1. [3, 15]

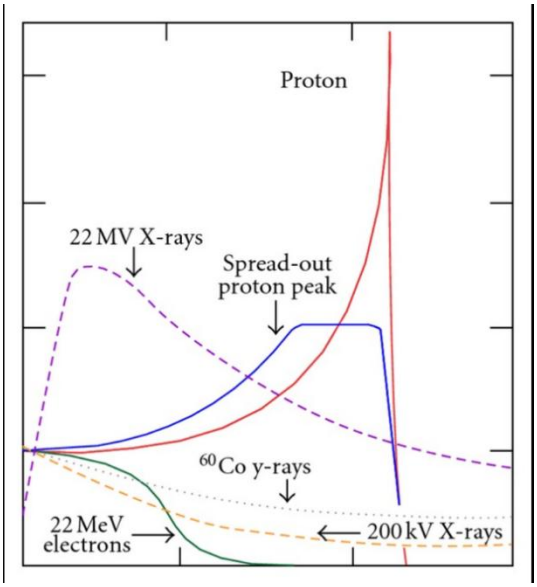

Figure 1: Bragg peak and Spread-Out Bragg Peak (SOBP) for a proton beam in comparison with photon and electron dose distributions from [Cianchetti, M, 2012]

1.3.1 Proton interaction with matters

In contrast to photon, a proton is a particle. There are some predominant types of interactions of protons in a matter: Coulombic interactions with atomic electrons, Coulombic interactions with the atomic nucleus and nuclear reactions. In most cases, protons maintain a nearly straight trajectory as they possess a mass that is 1836 times greater than that of electrons. However, a small number of protons will interact with nucleus and deflect from its original straight-line trajectory. Changes in the paths of protons can cause scattering or variations in dose distribution, which will affect the precision in proton therapy.

1.3.2 Energy loss rate and range

The stopping power of proton is defined as the quotient dE and dx. $S = \frac{\mathrm{dE}}{\mathrm{dx}}$ is the equation to express the stopping power. If neglect mass density of absorbing material, mass

stopping power is shown as $\frac{S}{\rho} = \frac{dE}{\rho dx}$, which is the simplest but still remarkably accurate. Stopping power is defined for a beam, not for a particle.

The path of most protons in matter is nearly straight. The Continuous Slowing Down Approximation (CSDA) Range for protons refers to the theoretical distance a proton travels in a material before coming to a stop. The range can be calculated by the formula:

$$R(E) = \int_0^E \left(\frac{dE'}{dx}\right)^{-1} dE' \cong \sum_0^E \left(\frac{dE'}{dx}\right)^{-1} \triangle E' \qquad [Eq.\ 1]$$

1.4 Biological Effect of proton therapy

Relative Biological Effectiveness (RBE) is defined as the ratio of dose required to produce the same biological effect between a radiation beam (often charged particles) and a reference radiation, usually defined as 250 kVp X-rays. RBE depends on the conditions under which the effect is measured. In clinical standards, the RBE of proton beam is consistently regarded as 1.1. Paganetti's review paper [24] presents collected clinical data indicating that the RBE at the entrance of the beam is 1.1, increases to 1.3 at the distal edge, and reaches 1.7 in the distal fall-off region. This represents a significant development of proton therapy, as a higher RBE corresponds to an enhanced ability to destroy cancer cells. Yet, the adoption of a variable RBE value in clinical practice has not occurred for three reasons:

1. The uncertainty of The RBE values in a clinic context.
2. The inability to incorporate a variable RBE into commercial treatment planning systems.
3. The limited evidence supporting variable RBE.

Oxygen is a major biological factor. For low LET radiation, like photon and gamma ray, the regions of tumor that are hypoxic (lack of oxygen) are more radioresistant. Oxygen rapidly converts the free radicals generated after irradiation into harmful peroxide radicals, which are precursors to DNA damage. The oxygen enhancement ratios (OERs) of photon beams are lower than those of proton beams. Proton beams have an advantage in treating radiation-resistant hypoxic cells compared to X-ray treatment. [4]

1.5 The history of proton therapy

1.5.1 Passive scattered proton therapy (PSPT)

In passive scattered proton therapy, mono-energy proton beam is generated from machine, and then pass through energy modulator wheel, which rotates at a typical frequency of 10 Hz. All energies are created within one wheel cycle. To provide a uniform beam, the multiple-energetic beam is spread out laterally by one scatter for small target size and two scatter for larger target size to be a uniform beam. The maximum field size of the spread proton beam can be up to 25 cm diameter. Collimators in passive scattered proton therapy is to shape lateral field size. Range compensator ensures proton beam will stop at the distal part of tumor area.

The dose distribution of passive scattered proton therapy is depicted in Figure 2. At the distal part of the tumor, there is no exit dose; however, in the proximal part of the tumor area, some extra dose extends beyond the tumor boundaries. The reason is that the spread out Bragg peak plateau of the beam is determined by the largest cross-section of the target volume, so some normal tissue near the proximal part of tumor will receive the uniform dose as target area. [15]

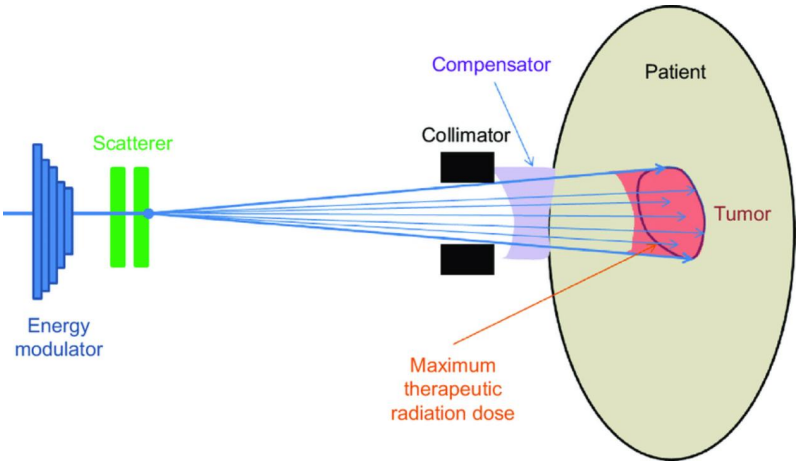

Figure 2: Illustration of passive scattering delivery method in proton therapy from [Wang D. (2015)].

1.5.2 Active pencil beam scanning

Active pencil beam scanning does not require energy modulator wheel, scatters, compensator or collimator. There are two pairs of magnets to scan the fine pencil beam. The range of each pencil beam is adjusted through energy switching in the energy selection system. Active pencil beam scanning can reduce the risk of secondary cancer due to reduced neutron radiation created compared to the passive scattered proton therapy. Pencil beam scanning also provides high quality of the dose distribution, avoiding unnecessary dose to proximal normal tissue. [15]

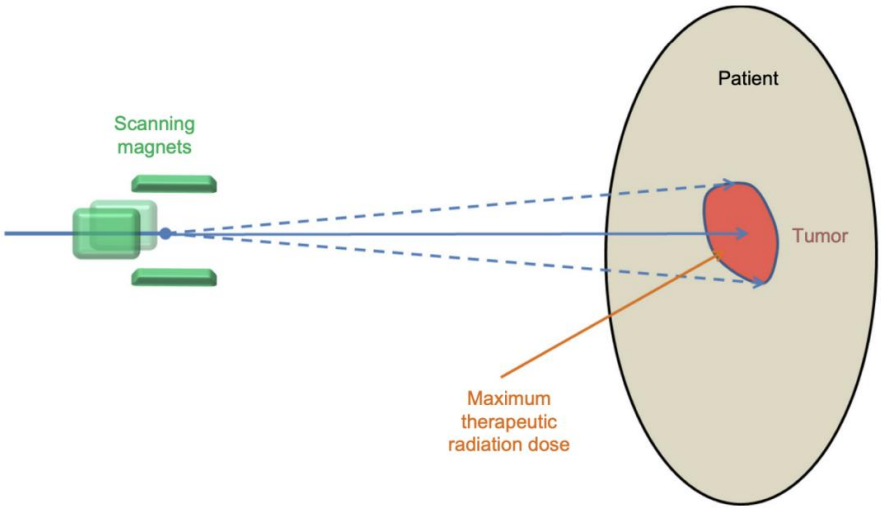

Figure 3: Illustration of pencil beam scanning delivery in proton therapy from [Wang D. (2015)].

The degree of freedom provided by pencil beam scanning is the fundamental of the development of intensity modulated proton therapy (IMPT).

1.5.3 Intensity Modulated Proton Therapy

Intensity-modulated proton therapy (IMPT) is an application of active pencil beam scanning. Like intensity-modulated photon therapy, IMPT not only enables precise coverage of complex tumor morphologies but also significantly reduces radiation exposure to surrounding normal tissues and organs at risk (OARs), offering a distinct advantage.

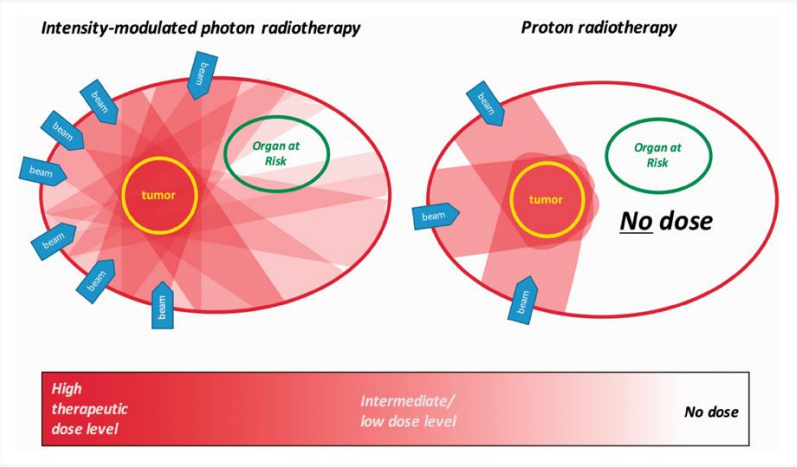

Figure 4: Comparison between proton arc therapy and IMPT from [Depuydt T, 2018].

However, there is one limitation of IMPT: range uncertainty. Range uncertainty can arise from organ motion, setup errors and stopping ratio estimation uncertainty. These uncertainties are reflected in proton treatment plans by not knowing where protons stop within the body.

1.5.4 Proton arc therapy

Proton arc therapy is becoming clinically available, delivered as active pencil beam scanning. Its advantage over IMPT is the demonstrated superior sparing of normal tissue in adults for extra-cranial tumor sites.

The physical properties of protons are different from photon, in terms of linear energy transfer and relative biological effectiveness. LET increased at the end of proton range, potentially leading higher dose to normal tissues near distal part of tumor. It can be addressed by the choice of angle beams and increasing the number of beams. These two solutions can reduce LET hotspots at organs at risk.

Proton arc therapy enhances the dose gradient through the use of multiple beams. The dose gradient, defined as the average distance between two isolines, reflects the steepness of the

dose distribution. [10] This results in a rapid dose reduction at the tumor's edge, thereby preserving the surrounding normal tissues. However, this advantage diminishes when the number of beams reaches 12. [11]

Spot-Scanning Proton Arc (SPArc) Therapy is a novel, robust, and delivery-efficient technique. The method integrates control point redistribution, energy layer redistribution, energy layer filtration, and energy layer resampling. Initially, SPArc begins with coarse sampling using eight static beams. In the control point resampling step, two new adjacent sub-control points replace the original control point. The increase in the number of control points after control point redistribution reduces the number of energy layers per control point and results in a more even distribution of energy layers. Energy Layer Switch Time (ELST) is a major factor affecting total delivery time in SPArc therapy. Energy layer filtration and resampling can reduce the number of energy layers while maintaining plan quality and treatment efficiency.[25]

To reduce the total treatment delivery time, minimizing the number of energy layers in each control point is a reasonable approach. K-means clustering analysis and particle swarm optimization can decrease the total treatment delivery time by organizing energy layers in descending order within each sector and in ascending order between two sectors. Particle swarm optimization is employed to reduce the number of energy layers at each control point while maintaining the total spot coverage of the target. The objective function of particle swarm is $f_1 = \alpha T - (1-\alpha)P = \alpha \sum_i Ti - (1-\alpha) \sum_i Pi$. α is set to 0.9 to minimize the energy layer switch time and maximize spot coverage. [26]

1.6 matRad

1.6.1 Computational Platform

MatRad [16] is an open-source toolkit specifically designed for radiation treatment planning. Developed entirely in Matlab, it supports the simulation of the entire process of photon, proton, and carbon ion therapy. This includes tumor segmentation, machine data, planning parameters, inverse planning, and dose distribution calculation.

1.6.2 Proton machine data

MatRad comes with a comprehensive database that includes machine data for 114 different beam energies, ranging from 31.72 Mega-electron Volts (MeV) to 236.1 MeV. For each energy level, the database details its range, peak position, and Linear Energy Transfer (LET).

Lateral beam broadening is due to multiple Coulomb scattering calculated by Molière's formalism. Molière's formalism is used to predict the scatter angle, called as characteristic angle θM, reflecting the average angle at which particles deviate from the original path during the scattering process. For some protons passing through thick targets, the characteristic angle appearances to level off.

1.6.3 Patient data

The matRad software toolkit has anonymized patient and phantom data, including prostate, liver, head and neck, and TG119 C-shape stored in a custom Matlab file format. Each case data has computed tomography (CT) images (file: ct) as well as segmentations and predefined treatment planning parameters (file: cst).

1.6.4 Treatment Parameters

The treatment parameters are defined within a Matlab structure, denoted as 'pln'. This structure stores the choice of radiation modality, the number of beam, the number of gantry

angles, the number of couch angles, bixel width, the isocenter, biological optimization and dose grid resolution.

1.6.5 Beam Geometry and Delivery

Beam geometry is within a Matlab structure (stf), including the details of gantry angle, couch angle, Source-to-Axis Distance (SAD). The ‘stf’ structure details each beams’ details, including the number and position of ray of each beam, and energy layers. It also includes details about range shifters which adjusts the proton beam's energy for more precise.

1.6.6 Dose Calculation

After establishing the beam configuration, the next steps are 3D dose calculation and inverse fluence optimization. The 3D dose calculation involves a detailed process that calculates the dose for each pixel in every beam, using comprehensive looping through all elements. In this context, the Relative Biological Effectiveness (RBE) is consistently set at 1.1. Machine data provide the Linear Energy Transfer (LET), essential for accurate particle dose calculations. The optimization of inverse fluence is efficiently conducted using IPOPT optimization, known for its effectiveness in handling complex optimization tasks.

1.6.7 Objective function and Constraints

Objective functions and constraints are used in matRad, a radiation treatment planning toolkit, for dose distribution optimization. Objectives include minimizing the squared deviation of the actual dose from the prescribed dose, penalizing under and over-dosage, targeting mean dose values, and considering the Equivalent Uniform Dose (EUD) and Dose-Volume Histogram (DVH) criteria. Constraints ensure doses stay within minimum and maximum limits for safety and effectiveness. These mathematical formulations are critical to fine-tuning treatment plans to target tumors precisely while protecting healthy tissues.

1.7 Motivation and Objective

Shortening the delivery time of proton arc therapy can enhance efficiency. My thesis aims to streamline the process by reducing the number of energy layers to just one for each beamlet and by using range shifters, thereby eliminating the time-consuming energy switching caused by magnetic hysteresis in active pencil beam scanning. This approach sets a single maximum energy for each ray, optimizing therapy time.

2. Method and Material

2.1 Multiple-energy layer to Mono-energy layer optimization (Mono energy optimization)

In proton therapy, the utilization of multiple energy layers within a single ray is to ensure comprehensive tumor coverage and enhance the quality of the treatment plan. However, switching between energy levels in proton therapy equipment is time-consuming. According to the specific from the IBA proton machine, descending one energy level requires 0.6 seconds and elevating energy layer needs 5.5s. [12] It is necessary to reduce energy layer of each ray to enhance delivery efficient.

In-house particle swarm optimization was employed to select the optimal energy layer for each ray.[13] Let i represent the i-th beam, and j the j-th ray. $P_{i,j}$ denotes the spot coverage of the j-th ray within the i-th beam. Building on particle swarm optimization, the iterative optimization algorithm cycles through all rays and beams to identify the maximum spot coverage. For each ray across all beams, it evaluates different energy layers, computes the coverage, and updates the maximum coverage along with its associated energy layers. The method for calculating spot coverage involves initially determining the total volume of the target, then identifying the number of points corresponding to that energy and computing the volume of that energy layer. Consequently, $P_{i,j}$ is ratio of the volume of the j-th ray's energy layer in the i-th beam to the total target volume. The objective function for iterative optimization algorithm is as follows:

$$f = \sum_0^i \sum_0^j \mathbf{P}(i, j) \qquad [Eq.2]$$

When the optimal energy layer for each ray is selected, other energy layers are discarded, along with the spots deposited by these energy layers. The number of spots decreased significantly.

The optimal energy levels for all rays are compiled into an energy list, which will serve as the predetermined energy layers for further calculations or processes.

2.2 Set the machine maximum energy to all rays

Setting the machine's maximum energy for all rays can eliminate the energy switch time during treatment. However, the penetration depth of the maximum energy proton beam will exceed the patient's body, necessitating the use of an energy degrader to reduce the energy from the maximum level to the optimal level.

2.3 Range shifter design

The selected material for the range shifter is methyl methacrylate (PMMA), recognized for its density of 1.2 g/cm³. The thickness of the range shifters is determined using the stopping power, the maximum energy, and a predetermined energy level. The stopping power data can be obtained from the National Institute of Standards and Technology (NIST) website. Subsequently, the formula presented in the introduction section is applied. An illustrative example is provided in the figure below.

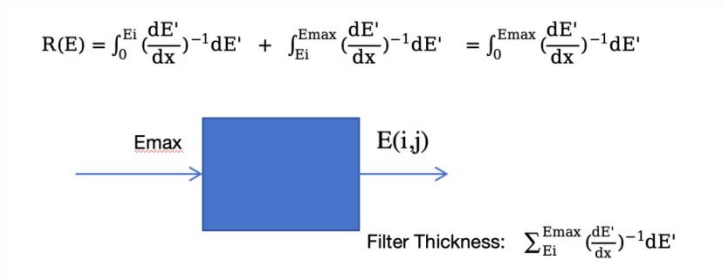

Figure 5: An example of how to calculate the thickness of a range shifter required to reduce energy from the maximum to a specific level.

The Source-to-Surface Distance (SSD) is established at 1000mm, with the patient positioned at the isocenter. The bases of the range shifters are mounted onto the gantry of the machine. For the 72 beams required in each case, 72 range shifters are arranged in a circular array, with each one's apex directed towards the isocenter.

In matRad, scatter caused by the range shifter is accounted for with specific steps to calculate this effect. Scatter results from multiple Coulomb interactions with atomic nuclei. Sigma (σ), representing the proton beam's width, changes as the proton beam passes through material, following a defined equation.

$$\sigma^2_m(z,E_0) = \int_0^z dz' \frac{d\theta^2_m}{dz}(z', E_0)(z-z')^2 \quad [Eq.\ 3]$$

$$\theta^2_m(z, E_0) = C_1^2(1 + C_2 log \frac{1}{L_R^m})^2 \frac{1}{L_R^m} \int_0^z dz' \frac{1}{4E^2_m(z')} \quad [Eq.4]$$

$$\sigma^2_m(z,E_0) \approx \sigma^2_m(\frac{z}{S_{mw}},E_0) * (F_{mw})^2 \quad [Eq.\ 5]$$

Where z and z' are depths, E_0 is the initial energy, θ average deflection angle at depth z, the lateral fluence at coordinates (r, z) and initial energy E_0 is denoted as $Lm(r, z, E_0)$, F_{mw} is introduced as a scaling factor, S_{mw} is the ratio of stopping power of the material to water, C_1^2 and C_2 are parameters.

2.4 Higher energy layer selection optimization (higher mono energy optimization)

The previous iterative optimization algorithm was effective without incorporating range shifters. Nonetheless, the introduction of range shifters alters the proton beam's trajectory due to the interactions between protons and the material. Thicker range shifters lead to increased scatter

and attenuation. To counter these effects, an additional characteristic, the normalized energy value, is introduced for the predetermined energy level, relative to the minimum and maximum energy levels across all beams. $E_{i,j}$ denotes the energy layer for the *j*-th ray within the *i*-th beam. Directly using the energy level as $E_{i,j}$ is impractical due to its wide range, especially since $P_{i,j}$, representing spot coverage, varies between 0 and 1. Therefore, $E_{i,j}$ must be normalized to align with the scale of $P_{i,j}$. To balance the significance of $P_{i,j}$ and $E_{i,j}$ in the optimization process, two parameters, alpha and beta, are utilized. In this project, both alpha and beta are set to 1, indicating that both $P_{i,j}$ and $E_{i,j}$ play crucial roles in the optimization.

The objective function for iterative optimization algorithm for selecting higher energy is as follows:

$$f = \alpha * \sum_0^i \sum_0^j (\mathrm{P}\ i, j\ ) + \beta * \sum_0^i \sum_0^j (\mathrm{E}\ i, j\ ) \qquad \alpha = 1; \quad \beta = 1; \qquad [Eq.6]$$

2.5 Evaluation

In this project, two or three beams of intensity-modulated proton therapy (IMPT) are used as the control group to compare plan quality. The dose grid resolution is 5x5x5mm^3. The details of IMPT is shown in Table 1.

Table 1: The prescription dose and beam arrangement for IMPT plans

Case	Prescription (Gy[RBE])	Fraction	Gantry angles	Dose calculation grid
Liver	45	25	270^0, 300^0, 320^0	5x5x5mm^3
Prostate	68	34	90^0,270^0	5x5x5mm^3
TG-119	50	35	0^0,90^0,270^0	5x5x5mm^3

Three representative cases (prostate, liver and TG-119 C-shape) were retrospectively selected for testing. The prescription dose, the number of fractions, gantry angle selection and the voxel of CT resolution are listed in Table 2. The dose grid resolution is 5x5x5mm^3.

Table 2: The prescription dose and beam arrangement for Mono-energy optimization

Case	Prescription (Gy[RBE])	Fraction	Arc Gantry Angle Selection	Dose calculation grid
Liver	45	25	Full arc with angle sampling frequency of 5 degrees	5x5x5mm^3
Prostate	68	34	Full arc with angle sampling frequency of 5 degrees	5x5x5mm^3
TG-119	50	25	Full arc with angle sampling frequency of 5 degrees	5x5x5mm^3

2.6 Plan quality evaluation

For plan quality evaluation, the dose-volume histograms (DVHs) of targets and important Organs at Risk (OARs) were generated to compare three IMPT plans and their corresponding three mono-energy with higher energy selection plans(higher energy optimization).

For dosimetric analysis, following indices were used:

For target volume:

D_{98} is the dose level received by 98% of the target volume, often used as an indicator of the near-minimum dose within the volume.

D_2 is the dose level received by the highest-dose 2% of the target volume, often used as an indicator of the near-maximum dose within the volume.

The homogeneity index was calculated using the following formula:

$$HI = \frac{D2-D98}{D\,prescription} * 100\% \qquad [Eq.\ 7]$$

Where D prescription is prescription dose.

Lower Homogeneity Index (HI) values indicate a more homogeneous dose distribution within the target. [14]

Conformity indices (CI) is used to assess the degree of radiation dose coverage of the target area (typically a tumor) and the effectiveness of protecting surrounding normal tissues in a treatment plan. The formula of CI is show below.

$$CI = \frac{V\,T,ref}{V\,T} * \frac{V\,T,ref}{Vref} \qquad [Eq.\ 8]$$

Where VT is target volume, VT,ref is the target volume covered by reference isodose line. Vref is the total volume covered by the reference isodose line. A value equal of CI to 1 signifies an ideal situation.

2.7 Robustness analysis

Robustness is crucial in proton therapy due to range uncertainty, anatomical changes, and set-up displacement. Robustness is important is to ensure the accurate delivery of proton beams to the targeted tumor while minimizing exposure to surrounding healthy tissues. In this project, nine scenarios were used, including one nominal case, two range uncertainty cases by scaling the CT number by 3.5%, and six setup uncertainty cases by shifting the patient along with anteroposterior, superior-inferior, and mediolateral directions (3 mm for the TG-119 case and 5 mm for the rest).

The reference is IMPT plan. Dose volume histogram band (DVHB) is used to analyze the robustness of two plans. . The width of the bands for each anatomical structure reflects how much the volume receiving a specific dose could vary. Narrower bands suggest that the treatment is more robust meaning the dose delivered will be consistent despite these uncertainties. Wider bands indicate a greater potential variance in the dose that parts of the anatomy could receive.

3.Result

3.1 IMPT plan

This project uses two or three beams in the IMPT as the reference plan. The result of three cases will be presented in the following section.

3.2 Mono energy optimization

In this section, we use Dose-Volume Histograms (DVHs) exclusively to evaluate the quality of plans in relation to the IMPT plan, with the DVHs and corresponding dose distributions presented in the figures below.

This subsection discusses three cases to assess the quality of plans generated through mono-energy optimization. It has been observed that this approach has certain limitations, particularly concerning the dose in the target area and scatter due to range shifters. Consequently, a new method, termed "higher mono energy optimization," has been introduced to enhance plan quality. This improved method prioritizes higher energy levels for each ray, allowing for the use of thinner range shifters. This, in turn, reduces scatter and attenuation when compared to the original mono energy plan.

For the liver case:

The OARs, such as the heart and stomach in the mono-energy plan, receive a higher dose compared to the IMPT plan, affected by scatter due to range shifters. Additionally, targets in the mono-energy plan receive a lower dose than those in the IMPT plan at most target area, attributable to the attenuation and scatter from the range shifters. However, some target areas receive a higher dose, shown at figure6 (d). In this slice, the dose received by target of mono energy optimization is little higher than that of IMPT plan.

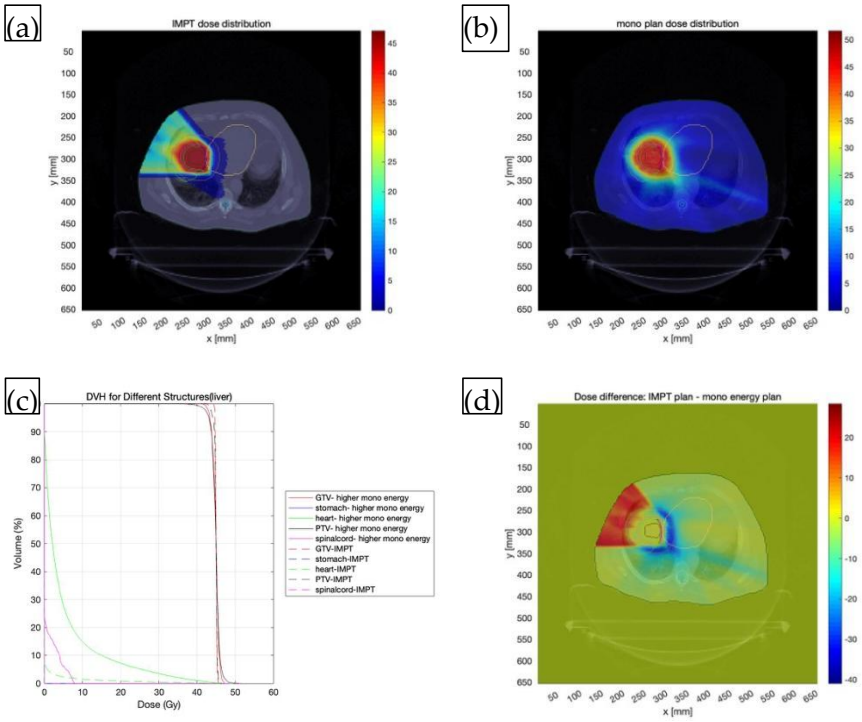

Figure 6: Dose distribution and dose difference between two plans

For prostate case:

The dose target of the mono-energy plan is lower than that of the IMPT plan, as visually evident in Figures 7(c) and (d). The dose difference between the IMPT plan and the mono-energy plan is approximately 3Gy in target area of this dose slice. Furthermore, the dose received by the rectum in the mono-energy plan exceeds that in the IMPT plan.

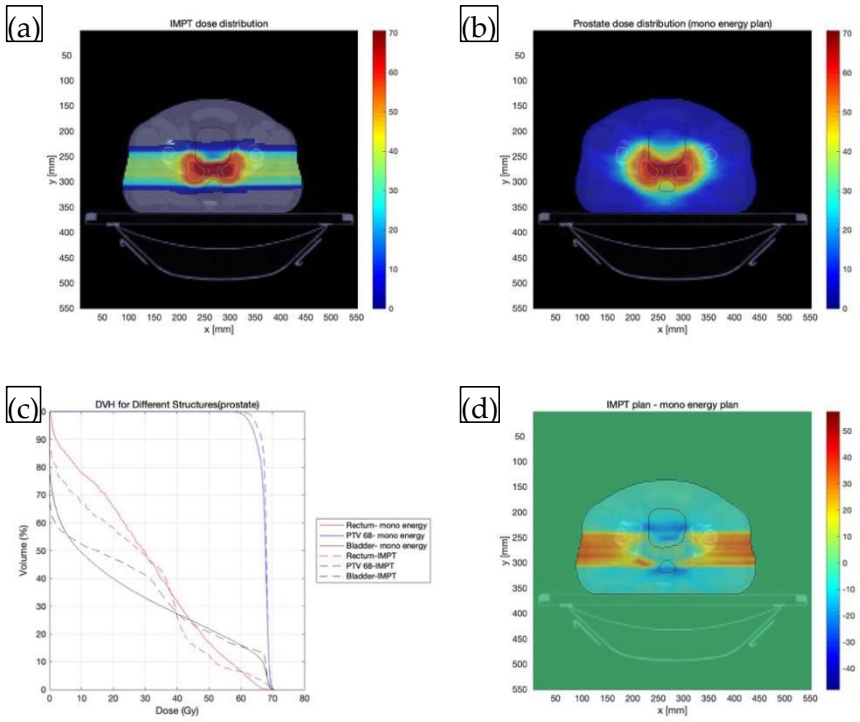

Figure 7: Dose distribution and dose difference between two plans

For TG-119 Case

In the mono-energy optimization, 20% of the target volume receives a lower dose compared to the IMPT plan, as illustrated in Figure 8(c). The core in the mono-energy optimization receives a higher dose than in the IMPT plan, which could be attributed to increased scatter and the use of additional beams in arc therapy.

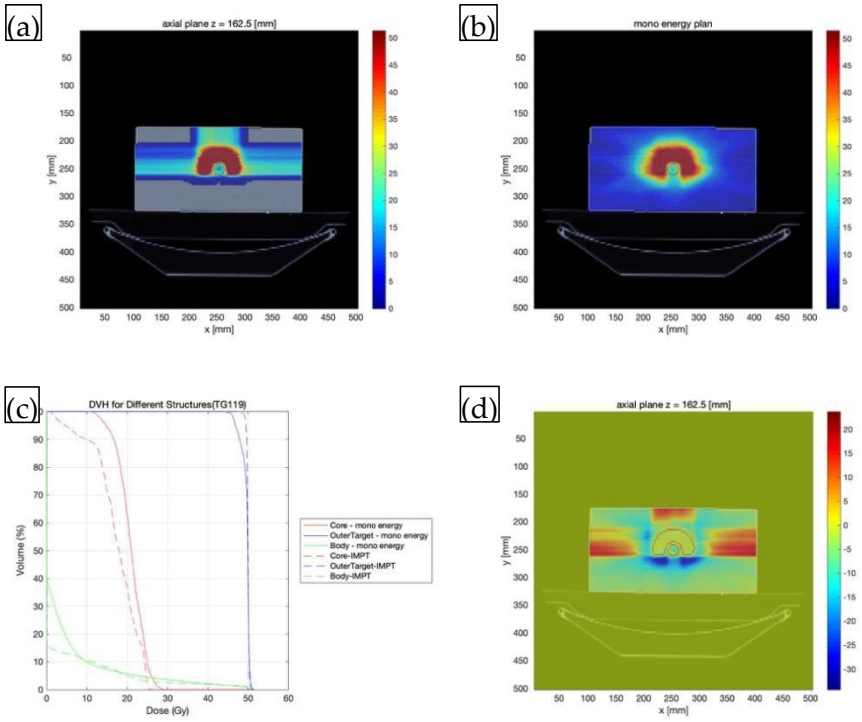

Figure 8: Dose distribution and dose difference between two plans

3.3 Range shifter

In three cases, there are 72 beams, which correspond to 72 range shifters. These shifters are designed in a circular layout. Each beam consists of multiple rays, with each ray having a specific height for its range shifter. The example of one angle's range shifter is shown in figure 9.

The blue points in 3D space represent the positions of each ray from the Beam's Eye View (BEV). A range shifter is comprised of many columns of different heights, with each column corresponding to a specific ray.

The 72 range shifters are arranged in a circular formation around the patient. The distance between the isocenter and the base of the range shifters is determined by the maximum height of the range shifters.

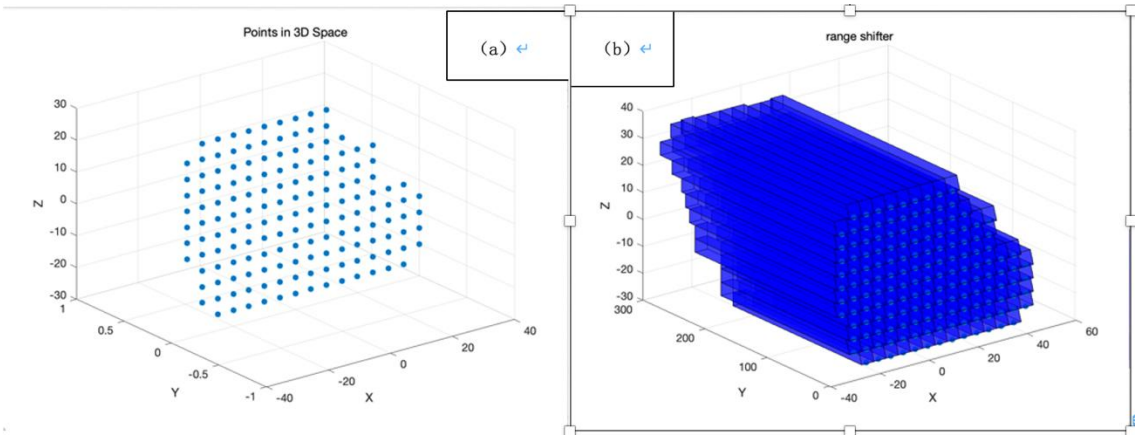

Figure 9: (a) The position of each ray. (b) The range shifter height for each ray.

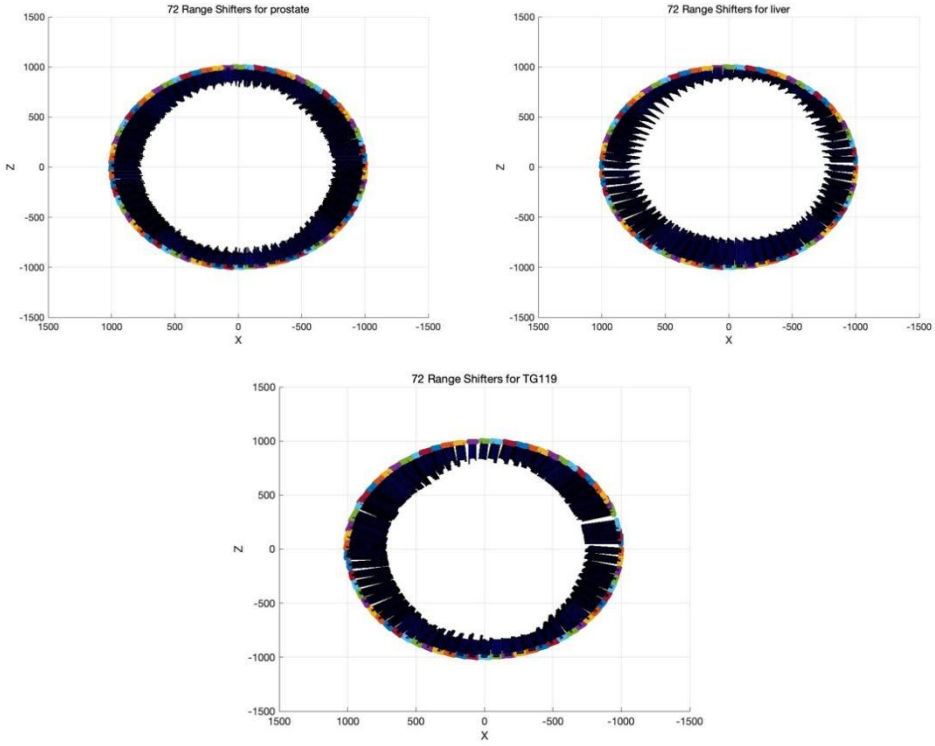

Figure 10: The display of range shifters for three cases

3.4 Higher mono energy optimization

Compared to mono-energy optimization, the height of range shifters in this method is smaller, resulting in less scatter and attenuation caused by the range shifter. The results show reduced dose in OAR areas and increased dose in target areas.

Prostate Case:

Compared to the mono-energy optimization method, higher energy optimization shows less scatter dose in areas beyond the target area. In Figure 10(d), this method decreases the dose by 5-30 Gy in most areas beyond the target area. In Figure 10(c), the higher energy mono-energy method provides a higher dose (around 4 Gy) in this dose slice within the target area.

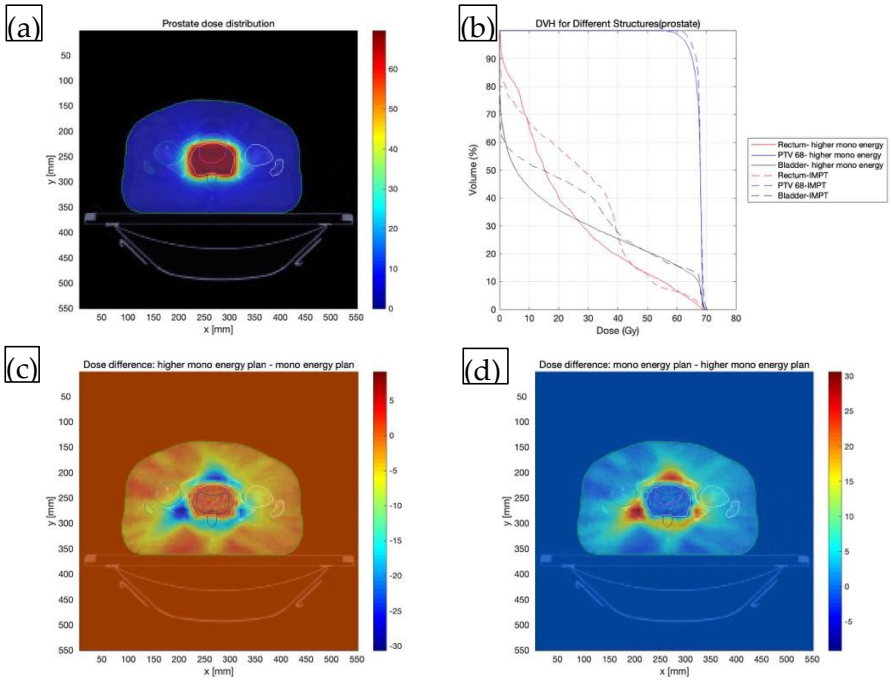

Figure 11: Dose distribution and dose difference between two plans

For Liver case:

Compared to the mono-energy optimization method, higher energy optimization shows less scatter dose in areas beyond the target area. In Figure 12(d), this method decreases the dose by 2-10 Gy in most areas beyond the target area. In Figure 12(c), the higher energy mono-energy method provides a higher dose (around 2 Gy) in some areas within the target area.

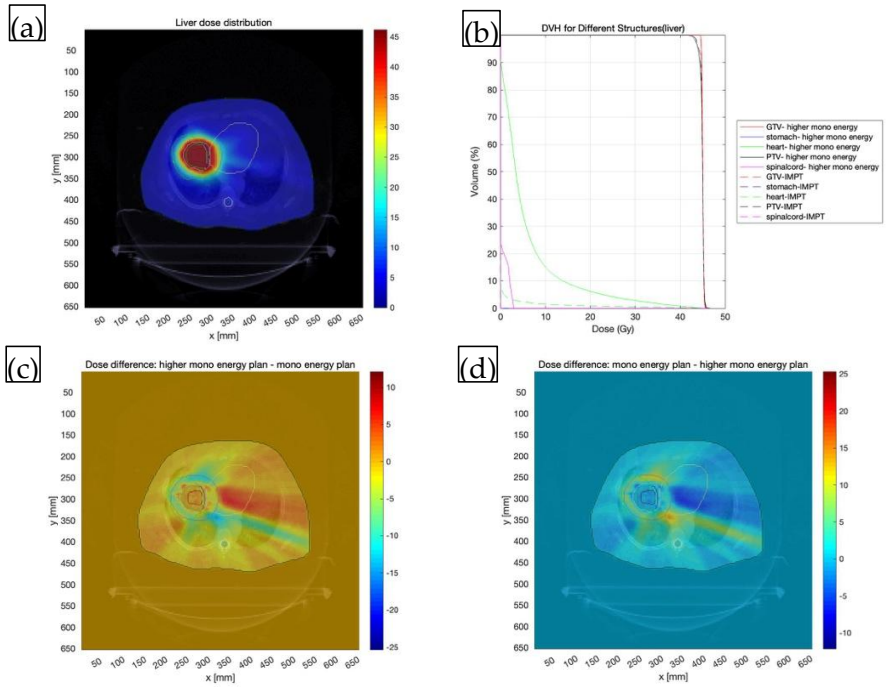

Figure 12: Dose distribution and dose difference between two plans

For TG-119:

Compared to the mono-energy optimization method, higher energy optimization shows less scatter dose in areas beyond the target area. In Figure 13(d), this method decreases the dose by 2-15 Gy in most areas beyond the target area. In Figure 13(c), the higher energy mono-energy method provides a higher dose (around 2 Gy) in some areas within the target area.

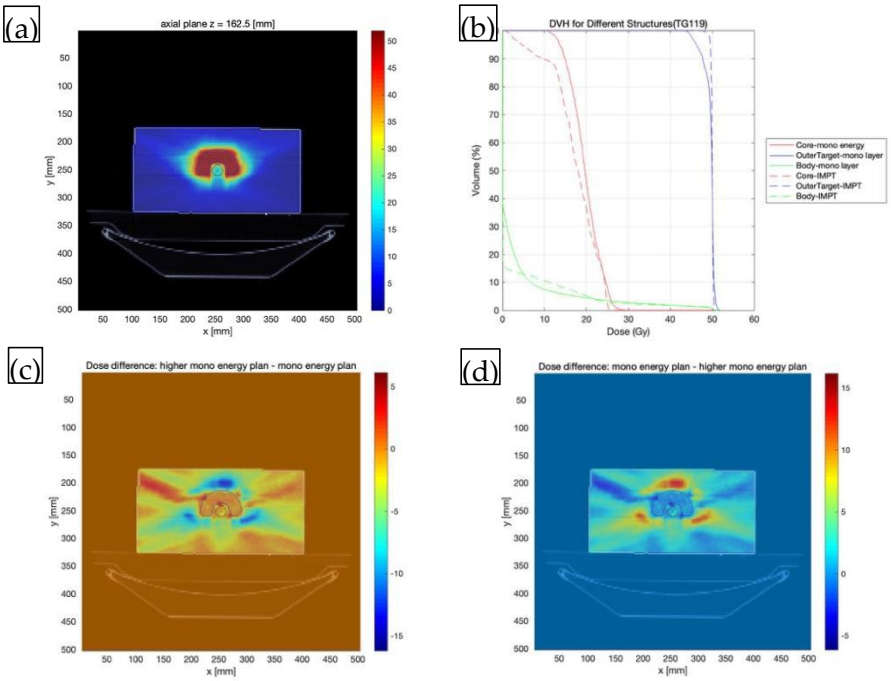

Figure 13: Dose distribution and dose difference between two plans

3.5 The delivery time

In the context of prostate cases, the treatment duration is approximately 360 seconds. With the gantry speed maintained at roughly 1 degree per second, it implies that there is minimal to no time allocated for switching energy levels during the procedure.

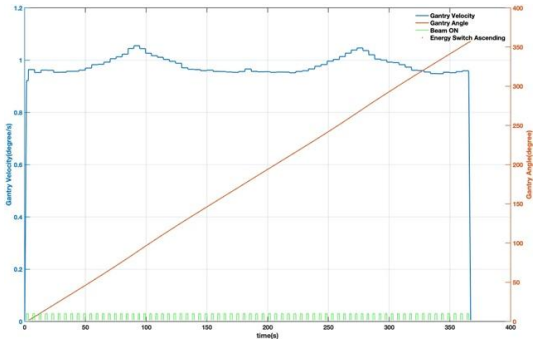

Figure 14: The delivery time of prostate case.

In the context of liver cases, the treatment duration is approximately 340 seconds. With the gantry speed maintained at roughly 1.1 degree per second, it implies that there is minimal to no time allocated for switching energy levels during the procedure.

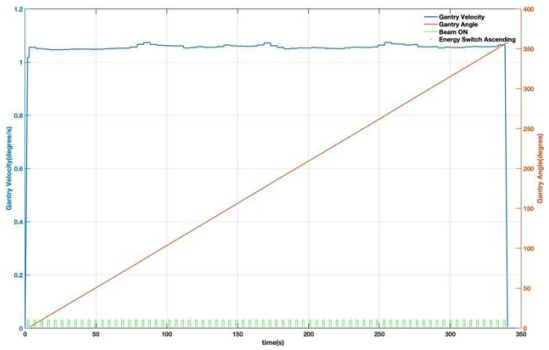

Figure 15: The delivery time of liver case.

In the context of liver cases, the treatment duration is approximately 380 seconds. With the gantry speed maintained at roughly 0.9 degree per second, it implies that there is minimal to no time allocated for switching energy levels during the procedure.

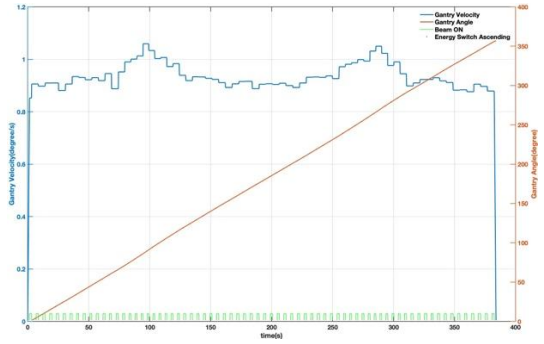

Figure 16: The delivery time of TG-119 Case.

3.6 Plan quality evaluation

The table presents a comparison between the plan quality of IMPT (Intensity-Modulated Proton Therapy) plans and higher mono-energy plans. The higher mono-energy plan is slightly inferior to the IMPT plan. However, it meets clinical acceptance criteria in most aspects.

Table 3: The plan quality of IMPT plan and higher mono energy plan

Case	Structure	Type	Clinic Constraints	3-beam IMPT	Mono-energy layer with range shifters
Prostate	PTV_68	D98%(Gy)	>68*0.95=64.6Gy	63.6Gy	60.89Gy
		D2%(Gy)	<68*1.07=72.76Gy	69.53Gy	68.97Gy
		CI		0.9150	0.8549
	Rectum	V_{40}	<30%	26.56%	19.45%
		V_{65}	<20%	4%	3.27%
	Bladder	V_{40}	<50%	27.65%	25.42%
		V_{65}	<25%	14.03%	12.59%
Liver	PTV	D98%(Gy)	>45*0.95=42.75Gy	43.58Gy	43.36Gy
		D2%(Gy)	<45*1.07=48.15Gy	45.56Gy	45.49Gy
		CI		0.9	0.88
		HI		2.7	3.4
	Spinal Cord	Max(Gy)	<8Gy	0	3.01Gy
	Heart	V_8	<15%	6.85%	20%
TG-119	PTV	D95%	>50	49.5Gy	46.25Gy
		D10%	<55Gy	50.46Gy	50.27Gy
	Core	D5%	<25Gy	24.76Gy	25.59Gy

3.7 Robustness analysis

For three cases, proton arc plans demonstrate better robustness compared to IMPT plans. The numerous proton beams are more resistant to various types of uncertainty.

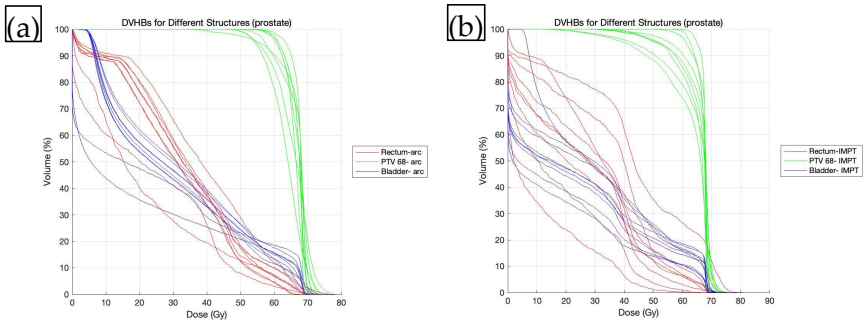

Figure 17: Robustness analysis for Prostate Case

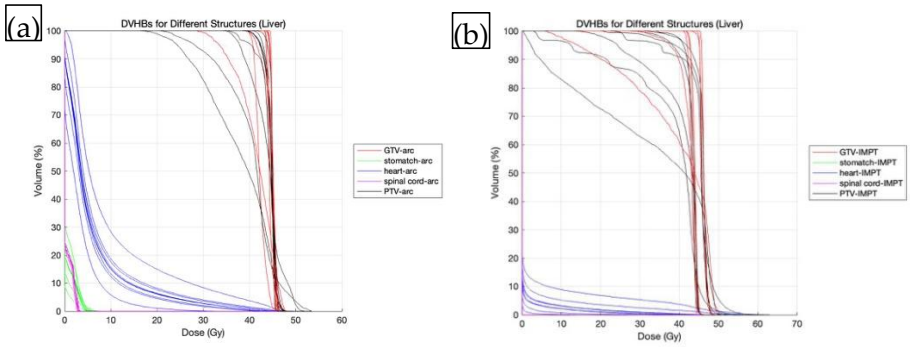

Figure 18: Robustness analysis for Liver Case

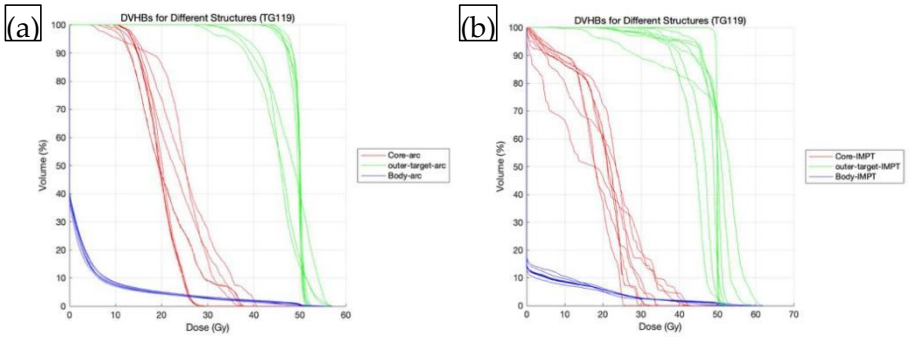

Figure 19: Robustness analysis for TG-119 Case

4. Discussion

4.1 The advantage of this project

This project benefits from the utilization of range shifters, which eliminates the need for energy switching time in the machine. Consequently, the treatment delivery time is reduced. Additionally, the stability of the gantry speed contributes to a faster delivery time. Among the three selected cases, no significant differences were observed, suggesting that the complexity of the treatment plan does not affect the delivery time. This could be attributed to the elimination of the need for energy switching.

4.2 Range Shifter design

It's impractical to position 72 range shifters around a patient in a circular arrangement for several reasons. First, the cost would be prohibitive since range shifters are typically manufactured using 3D printing, which can be expensive. Second, there's a risk of overlap, especially if the field size is large and the gantry angle spacing is narrow. This could lead to complications in the treatment delivery.

To tackle the challenge, the proposed method would involve manufacturing multiple flat slabs out of different materials, with each slab providing precise attenuation for specific beam paths. This strategy would refine the range shifter's design to cater to varying radiation attenuation demands without the need for numerous shifters. For scenarios requiring lower energy attenuation, slabs could be made thinner or selectively removed. Implementing this idea necessitates altering the number of slabs for each beam path, which poses a significant technical challenge, especially since the slab transition time needs to be within milliseconds.

4.3 Plan quality analysis

The dose deposition in the target area during proton arc therapy is slightly lower compared to the IMPT plan. Tumor size, shape, and location significantly impact the efficiency of the treatment planning system. For liver cases, the shape of liver tumors is regular, allowing the dose in higher mono-energy plans to be the same as that in IMPT plans. However, for the TG-119 and prostate cases, where the tumor shapes are irregular and the organs at risk are close to the target, irregular shapes or proximity to critical structures complicate achieving full coverage while protecting healthy tissue. Complex tumors demand advanced planning to ensure optimal treatment.

4.4 The limitations of matRad

All simulations are conducted using matRad. However, matRad is merely software and does not represent any specific proton machine. There is inevitably a gap between simulations and clinical applications. More machine data and clinical experiments are needed to bridge this gap.

4.5 Biological effect

In this project, the Relative Biological Effectiveness (RBE) of the proton beam is set at 1.1, without considering Linear Energy Transfer (LET) and variable RBE. It is necessary to take biological factors into account for more accurate results.

References

[1] Baskar, R., Lee, K. A., Yeo, R., & Yeoh, K.-W. (2012). Cancer and Radiation Therapy: Current Advances and Future Directions. International Journal of Medical Sciences, 9(3), 193–199. https://doi.org/10.7150/ijms.3635

[2] Baskar, R., Lee, K. A., Yeo, R., & Yeoh, K.-W. (2012). Cancer and Radiation Therapy: Current Advances and Future Directions. *International Journal of Medical Sciences*, *9*(3), 193–199. https://doi.org/10.7150/ijms.3635

[3] Chhabra, A., Langen, K., & Mehta, M. P. (2016). An overview of modern proton therapy. Chinese clinical oncology, 5(4), 48. https://doi.org/10.21037/cco.2016.05.06

[4] Gulliford, S. L., & Prise, K. M. (2019). Relative Biological Effect/Linear Energy Transfer in Proton Beam Therapy: A Primer. Clinical oncology (Royal College of Radiologists (Great Britain)), 31(12), 809–812. https://doi.org/10.1016/j.clon.2019.06.009

[5] Wang, X., Wang, X., Xiang, Z., Zeng, Y., Liu, F., Shao, B., He, T., Ma, J., Yu, S., & Liu, L. (2021). The Clinical Application of 3D-Printed Boluses in Superficial Tumor Radiotherapy. Frontiers in oncology, 11, 698773. https://doi.org/10.3389/fonc.2021.698773

[6] Vai, A., Molinelli, S., Rossi, E., Iacovelli, N. A., Magro, G., Cavallo, A., Pignoli, E., Rancati, T., Mirandola, A., Russo, S., Ingargiola, R., Vischioni, B., Bonora, M., Ronchi, S., Ciocca, M., & Orlandi, E. (2022). Proton Radiation Therapy for Nasopharyngeal Cancer Patients: Dosimetric and NTCP Evaluation Supporting Clinical Decision. Cancers, 14(5), 1109. https://doi.org/10.3390/cancers14051109

[7] Depuydt T. (2018). Proton therapy technology evolution in the clinic: impact on radiation protection. Annals of the ICRP, 47(3-4), 177–186. https://doi.org/10.1177/0146645318756252

[8] Moreno, A. C., Frank, S. J., Garden, A. S., Rosenthal, D. I., Fuller, C. D., Gunn, G. B., Reddy, J. P., Morrison, W. H., Williamson, T. D., Holliday, E. B., Phan, J., & Blanchard, P. (2019). Intensity modulated proton therapy (IMPT) - The future of IMRT for head and neck cancer. Oral oncology, 88, 66–74. https://doi.org/10.1016/j.oraloncology.2018.11.015

[9] Paganetti H. (2012). Range uncertainties in proton therapy and the role of Monte Carlo simulations. Physics in medicine and biology, 57(11), R99–R117. https://doi.org/10.1088/0031-9155/57/11/R99

[10] Sung, K., & Choi, Y. E. (2018). Dose gradient curve: A new tool for evaluating dose gradient. PloS one, 13(4), e0196664. https://doi.org/10.1371/journal.pone.0196664

[11] Toussaint, L., Indelicato, D. J., Holgersen, K. S., Petersen, J. B. B., Stokkevåg, C. H., Lassen-Ramshad, Y., Casares-Magaz, O., Vestergaard, A., & Muren, L. P. (2019). Towards proton arc therapy: physical and biologically equivalent doses with increasing number of

beams in pediatric brain irradiation. Acta oncologica (Stockholm, Sweden), 58(10), 1451–1456. https://doi.org/10.1080/0284186X.2019.1639823

[12] Gu, W., Ruan, D., Lyu, Q., Zou, W., Dong, L., & Sheng, K. (2020). A novel energy layer optimization framework for spot-scanning proton arc therapy. Medical Physics, 47(5), 2072–2084. https://doi.org/10.1002/mp.14083

[13] Wu, Q., Mohan, R., Morris, M., Lauve, A., & Schmidt-Ullrich, R. (2003). Simultaneous integrated boost intensity-modulated radiotherapy for locally advanced head-and-neck squamous cell carcinomas. I: dosimetric results. International journal of radiation oncology, biology, physics, 56(2), 573–585. https://doi.org/10.1016/s0360-3016(02)04617-5

[14] Cianchetti, M., & Amichetti, M. (2012). Sinonasal malignancies and charged particle radiation treatment: a systematic literature review. International journal of otolaryngology, 2012, 325891. https://doi.org/10.1155/2012/325891

[15] Wang, D. (2015). A critical appraisal of the clinical utility of proton therapy in oncology. Medical Devices (Auckland, N.Z.), 8, 439–446. https://doi.org/10.2147/MDER.S65594

[16] [16] Wieser, H. P., Cisternas, E., Wahl, N., Ulrich, S., Stadler, A., Mescher, H., Müller, L. R., Klinge, T., Gabrys, H., Burigo, L., Mairani, A., Ecker, S., Ackermann, B., Ellerbrock, M., Parodi, K., Jäkel, O., & Bangert, M. (2017). Development of the open-source dose calculation and optimization toolkit matRad. Medical physics, 44(6), 2556–2568. https://doi.org/10.1002/mp.12251

[17] Kang, M., Wei, S., Choi, J. I., Lin, H., & Simone, C. B. (2022). A Universal Range Shifter and Range Compensator Can Enable Proton Pencil Beam Scanning Single-Energy Bragg Peak FLASH-RT Treatment Using Current Commercially Available Proton Systems. International Journal of Radiation Oncology, Biology, Physics, 113(1), 203–213. https://doi.org/10.1016/j.ijrobp.2022.01.009

[18] Liu, G., Zhao, L., Li, X., Zhang, S., Dai, S., Lu, X., & Ding, X. (2023). A Novel Ultrahigh-Dose-Rate Proton Therapy Technology: Spot-Scanning Proton Arc Therapy + FLASH (SPLASH). International journal of radiation oncology, biology, physics, 117(3), 730–737. https://doi.org/10.1016/j.ijrobp.2023.05.012

[19] van de Water, S., Kooy, H. M., Heijmen, B. J., & Hoogeman, M. S. (2015). Shortening delivery times of intensity modulated proton therapy by reducing proton energy layers during treatment plan optimization. International journal of radiation oncology, biology, physics, 92(2), 460–468. https://doi.org/10.1016/j.ijrobp.2015.01.031

[20] Szymanowski, H., & Oelfke, U. (2002). Two-dimensional pencil beam scaling: an improved proton dose algorithm for heterogeneous media. Physics in medicine and biology, 47(18), 3313–3330. https://doi.org/10.1088/0031-9155/47/18/304

[21] Szymanowski, H., & Oelfke, U. (2003). CT calibration for two-dimensional scaling of proton pencil beams. Physics in Medicine and Biology, 48(7), 861–874. https://doi.org/10.1088/0031-9155/48/7/304

[22] Wei, S., Lin, H., Shi, C., Xiong, W., Chen, C. C., Huang, S., Press, R. H., Hasan, S., Chhabra, A. M., Choi, J. I., Simone, C. B., 2nd, & Kang, M. (2022). Use of single-energy proton pencil beam scanning Bragg peak for intensity-modulated proton therapy FLASH treatment planning in liver-hypofractionated radiation therapy. Medical physics, 49(10), 6560–6574. https://doi.org/10.1002/mp.15894

[23] Ding, X., Li, X., Zhang, J. M., Kabolizadeh, P., Stevens, C., & Yan, D. (2016). Spot-Scanning Proton Arc (SPArc) Therapy: The First Robust and Delivery-Efficient Spot-Scanning Proton Arc Therapy. International journal of radiation oncology, biology, physics, 96(5), 1107–1116. https://doi.org/10.1016/j.ijrobp.2016.08.049

[24] Paganetti H. (2014). Relative biological effectiveness (RBE) values for proton beam therapy. Variations as a function of biological endpoint, dose, and linear energy transfer. Physics in medicine and biology, 59(22), R419–R472. https://doi.org/10.1088/0031-9155/59/22/R419

[25] Ding, X., Li, X., Zhang, J. M., Kabolizadeh, P., Stevens, C., & Yan, D. (2016). Spot-Scanning Proton Arc (SPArc) Therapy: The First Robust and Delivery-Efficient Spot-Scanning Proton Arc Therapy. International journal of radiation oncology, biology, physics, 96(5), 1107–1116. https://doi.org/10.1016/j.ijrobp.2016.08.049

[26] Qian, Y., Dao, R., Liu, G., Li, X., Quan, H., & Ding, X. (2023). A novel planning framework for the efficient spot-scanning proton arc therapy via the particle swarm optimization (SPArc-particle swarm). Medical Physics, 50(6), e518–e519. https://doi.org/10.1002/mp.16525